Comparative Study of CO_2 and N_2 Foams in Porous Media at Low and High Pressure−Temperatures

Rouhi Farajzadeh,[†,‡] Alexey Andrianov,[‡] Hans Bruining,[†] and Pacelli L. J. Zitha*[,†,‡]

Department of Geotechnology, Delft University of Technology, Stevinweg 1, 2628 CN Delft, The Netherlands, and Shell International E&P, Kessler Park, 1, 2288 GS Rijswijk, The Netherlands

We report an experimental study of the behavior of CO_2 and N_2 foams in granular porous media using X-ray computed tomography. In the experiments either CO_2 or N_2 gas is forced through natural porous media initially saturated with a surfactant solution, a process known as surfactant-alternating-gas or SAG. The CO_2 was either under sub- or supercritical conditions, whereas N_2 remained under subcritical conditions at all experimental conditions. We found that CO_2 injection following a slug of surfactant can considerably reduce its mobility and promote higher liquid recovery at the experimental conditions investigated. Foaming of CO_2 builds-up a lower pressure drop over the core at both low and high pressures than N_2. Both gases require space to develop into foam. The space is longer for N_2 (larger entrance effect) and increases with increasing gas velocity. Moreover, the ultimate liquid recovery by CO_2 foam is always lower than by N_2 foam. The possible mechanisms explaining the observed differences in foaming behavior of the two gases are discussed in detail.

1. Introduction

The growing concern about global warming and shortage of energy supply has increased the interest in combined geological CO_2 storage and CO_2 flooding to enhance oil recovery (EOR).[1−3] Favorable characteristics of CO_2 include miscibility with oil, swelling, and the ensuing lowering of viscosity.[4−6] Even at immiscible conditions CO_2 can considerably reduce the oil viscosity and swell the oil volume leading to a significant improvement of oil recovery.[4−6] Nevertheless, due to its low viscosity and density, CO_2 segregates upwards, thus, overriding water (and eventually oil) and channels through high permeability streaks.[5,7] Foaming of CO_2 reduces its mobility and can potentially overcome these drawbacks.[5,8−10] Foam in porous media is a gas−liquid mixture with a continuous liquid phase wetting the rock, whereas a part or all of the gas is made discontinuous by thin liquid films called lamellae.[9,11,12] The mobility reduction of gas will result in a more favorable macroscopic sweep efficiency.[5,9,13] Even if the recovery is not improved the costs of handling of the gas will be reduced.[14]

Although the geological storage of CO_2 is considered as an attractive solution for global warming, the efficiency (or even feasibility) of the process is not yet established.[15] One major problem is the leakage of the injected CO_2 through the walls of abandoned wells or through the cap rock.[16] In this case foaming of CO_2 may temporarily hamper the leakage while other actions are considered.

There are two main injection strategies in EOR-field projects related to foam. These include co-injection of gas and liquid, and surfactant alternating gas (SAG) injection. In the first strategy the gas and the liquid are co-injected at a fixed ratio. The ratio between the gas flowrate and the sum of the gas and the liquid flowrates (total flowrate) determines the *foam quality*. The foam can also be generated outside the porous medium before injection, however; we categorize this strategy under the co-injection scheme. In the SAG scheme alternating slugs of surfactant solution and gas are injected and therefore foam is generated inside the porous medium (in situ generation).[9,17,18] The SAG foam is sometimes called *drainage foam* in the literature.[19] In a recent EOR application of the foam in the Norwegian Snorre field the SAG phase operations were conducted without any major problem while the co-injection was hampered by operational problems that resulted in unstable injectivity.[20,21] Moreover, the SAG process is similar to water alternating gas process (WAG) and requires little additional effort.[5,17−22] SAG injection minimizes contact between water and gas in surface facilities and piping which can be important when the gas, e.g., CO_2, forms an acid upon contact with water.[23,24] The laboratory study of Huh and Handy[25] also revealed that the gas-surfactant co-injection foam can completely block the porous medium under certain conditions, while this never occurs with the SAG foam. It was also shown that the mobility reduction factor is higher for co-injection foam than for SAG foam with the same gas flowrate.

While the co-injection foam has been the center of attention of many experiments [e.g., refs 26−31] there is only a little data on SAG foam.[18,32−34] Moreover, in most of the previous studies on foam flow in porous media the measured pressure drop became stationary only after 10−100 pore volumes of the injected fluids (liquid and gas). In these experiments the pressure drop does not increase significantly until the gas phase reaches the end of the initially surfactant saturated porous medium, a phenomenon that cannot be explained by the existing models.[35] Possibly, this happens due to the high gas flowrates or short length of porous media used in experiments. Indeed, the injected gas needs to travel inside the porous medium before it mixes with the available surfactant and foams. However, when the gas flowrate is high or the porous medium is short, the gas will breakthrough before making a strong foam. The gas will only start to form a strong foam if many pore volumes are injected in the laboratory setup and therefore the obtained results can only be representative of the initial stages of the injection process. It has been also observed that different gases behave differently, both in bulk[36−38] and porous media[18,39−42] experiments. Recently, Du et al.[27] experimentally showed that there is essential difference between CO_2 and N_2 foams in porous

* To whom correspondence should be addressed. E-mail: p.l.zitha@tudelft.nl.
† Delft University of Technology.
‡ Shell International E&P.

10.1021/ie801760u CCC: $40.75
Published on Web 04/08/2009

media. In their experiments the gases were co-injected with sodium dodecyl sulfate (SDS) solution with high gas flowrates. The differences were attributed to the dissimilar physical properties of the gases, mainly higher CO_2 solubility in water than N_2.

The choice of surfactant with respect to the injected gas, type of the porous medium, and chemical/physical properties of the fluids in the porous medium, for example, oil is an important key in the success of a foam injection process. A suitable surfactant should be capable of generating ample and stable foam in the presence of reservoir rock and oil at high pressures and temperatures. Furthermore, a successful surfactant should have low adsorption on the rock. Adsorption of the surfactant on the rock surface decreases the surfactant concentration and therefore shortens the distance that the surfactant will propagate into the oil reservoir before its concentration becomes too low to be effective in generating the foam.[43] The stability of foam in the presence of oil (often regarded as antifoam) is another challenge in the application of foam as an enhanced oil recovery (EOR) method. In general, the selected surfactant in EOR foam has to balance chemical costs against the expected gas mobility reduction, taking into account surfactant adsorption and foam-oil interaction.[44]

Alpha olefin sulfonate (AOS) surfactants have comparatively low adsorption on sandstones.[45] Moreover, AOS surfactants provide outstanding detergency, high compatibility with hard water, and good wetting and foaming properties with CO_2 even when the porous medium is partially saturated with oil. These properties make AOS surfactants an excellent candidate for (CO_2)-foam applications, for example, EOR projects that aim to produce more oil from underground reservoirs.

The purpose of this paper is two-fold. First we aim to add (high $P-T$) experimental data to the currently small database of SAG in the literature. Second, our goal is to study the effect of the gas type on the behavior of foam in porous media, at both low and high pressure−temperatures. Therefore, this paper focuses on describing the experiments when CO_2 or N_2 is injected into a porous medium that is initially saturated with a surfactant solution (SAG foam). Section 2 describes the experimental setup and the experimental procedures. Section 3 presents the experimental results for two sets of experiments. The first set of the experiments is performed at atmospheric pressure and a room temperature of $T = 20$ °C The second set of experiments is conducted at $P = 90$ bar and $T = 50$ °C. This condition is well above the critical point of CO_2. Section 4 provides detailed explanations of the differences observed in the experiments and investigates the relevant physical/chemical properties of gases affecting the foam behavior in the porous medium. Finally, we draw the main conclusions of this study.

2. Experimental Details

2.1. CT Imaging. The values of the CT scanner are measured in Hounsfield units (HU). The relationship between attenuation coefficient and HU is

$$HU_m = 1000\left(\frac{\mu_m}{\mu_w} - 1\right) \quad (1)$$

where μ_w displays the water attenuation coefficient: we obtain $HU_m = 0$ for water and $HU_m = -1000$ for air. The following equation is used to compute the liquid saturation, S_w, from the measured HU, eliminating the contribution of the rock by the subtraction:

$$S_w = \frac{HU_{foam} - HU_{dry}}{HU_{wet} - HU_{dry}} \quad (2)$$

where the subscripts foam, wet, and dry stand for the foam flow, solution saturated, and dry core conditions, respectively.

2.2. Materials. Chemicals. The surfactant used was alpha-olefin sulfonate, AOS (Stepan Company). This surfactant is anionic and was used as received without any further purification. The general structure of olefin surfactants is $R-SO_3^-Na^+$, where R represents the hydrophobic group. In our case the number of the carbon atoms in the surfactant structure is 12 and the molecular weight of the surfactant is $M_w \approx 273$ g/mol. A fixed active surfactant concentration of $c_{AOS} = 0.50$ wt % was used in our experiments. Sodium chloride (NaCl) was used to make the brine. The concentration of NaCl was a fixed value of 0.5 M (~3 wt %) in all experiments reported here. All solutions were prepared with deionized water (pH = 6.8 ± 0.1). To increase the CT attenuation of the solutions, 10 wt % of sodium wolframate (Aldrich, 99% purity) was added to the solutions.

Gases. The gases used to carry out the experiments were 99.98% pure CO_2 and N_2. The solubility of CO_2 in water is about 55 times higher than that of nitrogen.[46]

Porous Media. The porous medium used was consolidated, quasi-homogeneous, and quartz-rich Bentheimer sandstone. The main properties of the porous medium are presented in Table 1. The permeability was calculated from the pressure data of a single-phase (brine) flow (with a known flowrate) through the core and the porosity was determined from the CT data. The radius of the pore throats are mainly in the range of 10−30 μm.

2.3. Experimental Setup. The schematic of the experimental setup is schematically shown in Figure 1. It consists of four parts: injection unit (IU), test unit (TU), pressure controlling unit (PCU) and data acquisition system (DAS).

Injection Unit. To ensure the supply of the gas at a stable rate, the gas flow rate is controlled by using a high precision needle valve (for low-pressure experiments) and an ISCO pump (for high pressure experiments) and it is monitored by using a gas flow meter. A high precision double-effect piston displacement pump (Pharmacia P 500) is used to inject the brine and the surfactant solution at a constant rate.

Test Unit. In the test unit, the sample core is placed inside a cylindrical coreholder. The coreholder is made of poly(ethylene ether ketone) (PEEK) that combines good mechanical properties to a low X-ray attenuation. The geometry and structure of the core holder were designed to minimize beam hardening and scattering artifacts.[47] The core holder was placed vertically on the platform of the CT scanner apparatus and kept in place using a polymethyl methacrylate (PMMA) stand. The foam is introduced from the injection tube, and the liquid production is collected in a glass cup on an electronic mass balance. Two high precision pressure transducers locate at the inlet and the outlet to monitor the pressure drop along the core.

Pressure Control Unit. The pressure control part connects to the outlet of the core. By using a backpressure regulator and a manometer we can measure different pressures in the system. The data acquisition system records gas and liquid injection rates, pressures, and the liquid production data automatically. All experiments are conducted under isothermal conditions. The low pressure experiments are done at room temperature of $T =$ 20 °C and the high pressure experiments are performed at a constant temperature of $T = 50$ °C.

Most of the core-flood setup is positioned on the table of the CT scanner. The PEEK core holder is vertically placed,

Table 1. Properties of Sandstone Cores (Porous Media)

name	permeability [mD]	porosity [%]	diameter [mm]	length [mm]	pore volume [ml]	main composition
long core	1100 ± 100	22 ± 0.2	40 ± 1	170 ± 2	42.5 ± 0.5	quartz
short core	1100 ± 100	22 ± 0.2	40 ± 1	90 ± 2	22.5 ± 0.5	quartz

Table 2. Settings of the CT Scan Measurements

parameters	CT-scan settings
energy levels [keV]	140
current [mA]	250
slice thickness [mm]	3
number of slices	4
filter	B40-medium

perpendicular to the length of the table, to control the gravity segregation effects. The third generation SAMATOM Volume Zoom Quad slice scanner is used in our work. The main technical information about this machine has been provided elsewhere[26] and the imaging settings in our experiments are listed in Table 2. The X-ray tube of the CT scanner is operated at the voltage of 140 kV and the current of 250 mA. The thickness of CT slice is 3 mm, and one series of scan includes four slices. In the calculations the slice corresponding to the center of the core was used.

2.4. Experimental Procedure. Core Preparation. The cores were drilled from a large block and sawed to the dimensions specified in Table 1 using a diamond saw cooled with water. The cores were dried in an oven at 60 °C for at least 48 h. Then the cores were molded in Araldite glue to avoid production from the axial core sides. The core was then placed in a PEEK core holder. For pressure measurements inside the core, the pressure gauges were connected through a small hole drilled in the glue to the surface of the core. The connectors were also made of PEEK to reduce the beam-hardening effects of X-ray beam.

Before starting the experiments all of the connections in the setup were checked for possible leakages by keeping the setup under high pressure and monitoring the measured pressures.

Core Saturation. The core was flushed with CO_2 for at least 30 min to replace the air in the system. Afterward, at least 20 pore volumes of brine with the flowrate of $q_w = 2$ ml/min were injected to the system while the backpressure was set $P_b = 20$ bar. Therefore, all CO_2 present in the core is dissolved into the brine and carried away. This is confirmed by CT images.

Surfactant Injection. After the core was saturated with the brine, 1 pore volume of the surfactant was injected ($q_s = 2$ ml/min) to the porous medium. The adsorption of AOS surfactant on Bentheimer sandstone is very low.[45] Moreover, 1 wt % of AOS is well above its CMC value[44] and therefore, injection of 1 PV of surfactant would be sufficient to satisfy the rock adsorption.

Foam (Gas) Injection. The gas is injected into the core previously saturated with the surfactant solution (SAG foam).

3. Results

3.1. Low Pressure Foam Development. a. CT Scan Images. Figure 2 presents the CT images of the central part of the CO_2 and N_2 experiments, respectively. The time of each image is also shown in terms of the dimensionless time of pore volumes, *PV*, which is the ratio of the cumulative volume of injected fluids (in these experiments only gas) to the volume of the pore space in the porous medium. In these experiments the gas (CO_2 or N_2) was injected with a flowrate of 0.5 mL/min to the core initially saturated with 1−2 PV of the surfactant solution (SAG scheme). The blue and red colors represent the gas and the liquid phases, respectively. The general features of these experiments (foam advance) are similar to foam experiments in which the surfactant solution and the gas are co-injected into the porous medium.[27] For both CO_2 and N_2, the images show a front-like displacement of the aqueous phase by foam. Three regions can be distinguished in both experiments along the flow direction: (1) an upstream region which is characterized by low liquid saturation, (2) a region downstream of the foam front where the liquid saturation is still unchanged and equals unity, and (3) a frontal region characterized by a mixing of flowing foam and liquid and exhibits fine fingering effects. The extent of the fingering behavior is caused by the local rock

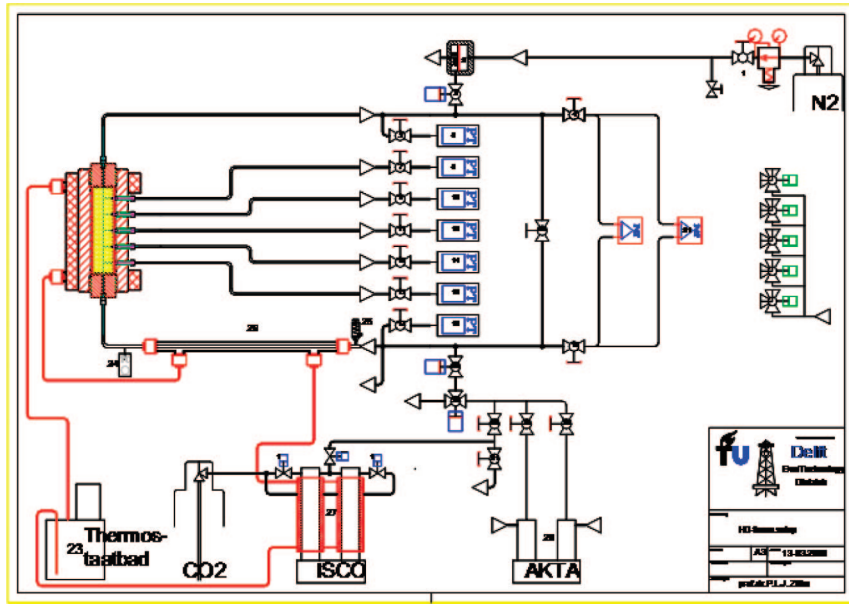

Figure 1. Schematic of the foam setup: It consists of four major units: injection unit (pumps), test unit (the porous medium), pressure controlling unit, and data acquisition system (not shown in this Figure).

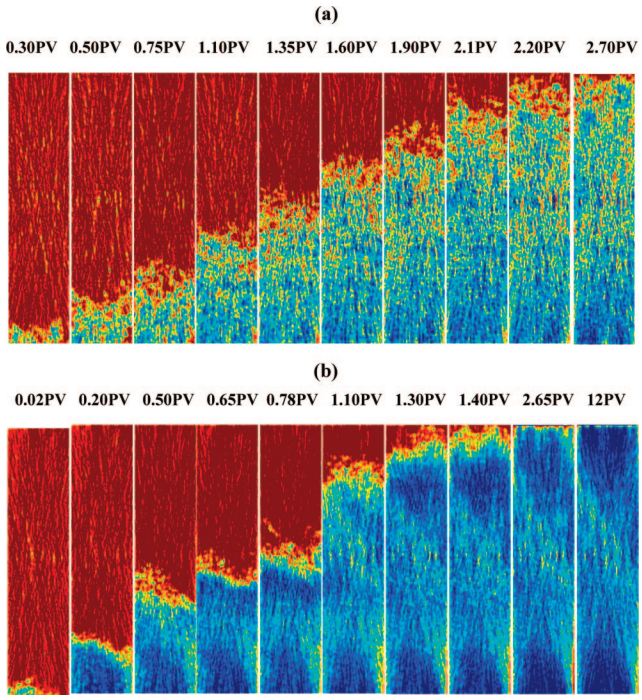

Figure 2. CT images of (a) CO_2 and (b) N_2 foam flow (blue) in a porous medium initially saturated with surfactant solution (red) at $P = 1$ bar and $T = 20$ °C ($q_g = 0.5$ mL/min). The time of each image is shown in pore volumes of the injected gas.

heterogeneity[26,28] and apparently depends on the type of the foamed gas (foam strength).

Nevertheless, a closer examination of the images reveals the considerable differences between CO_2 and N_2 foams. About 0.30 PV of CO_2 is injected before the gas penetrates the core and becomes visible in the images while N_2 becomes visible much more rapidly as the gas penetrates the core immediately displacing the liquid. This is possibly due to the higher solubility of CO_2 in water. The upstream region of CO_2 foam front is less blue indicating higher water content compared to the upstream region of N_2 foam. However, similar to N_2 foam, as the foam front progresses in the core, the gas sweeps parts of the remaining liquid from the upstream region toward the outlet. In the frontal region, N_2 foam is sharper than CO_2. Finally the higher solubility of CO_2 in the aqueous phase results in its substantially delayed breakthrough. The gas breakthrough takes places at a time between 1.30 and 1.70 PV for N_2 foam while the foamed CO_2 breaks through at a time slightly larger than 2.20 PV.

The amount of CO_2 that can be dissolved in water can be estimated by Henry's law. The solubility of CO_2 in water is ~38.4 mol/m^3 at our experimental condition. Using the CT images the volume of water that gas has met was estimated at each *PV* and then the amount of dissolvable CO_2 was calculated. The results are summarized in Table 3. In these calculations the possible effect of surfactant micelles on CO_2 solubility is disregarded. It turns out that the amount of dissolved CO_2 is considerable and therefore the effect of water solubility cannot be neglected.[27] Indeed, considering also some dead volume in the system, more than 1 PV of the injected CO_2 is required to saturate the liquid before it can form foam.

b. Saturation Profiles. To quantify the evolution of the liquid saturations, S_w, over the entire core, the CT data of the obtained images were converted to water saturation profiles using eq 2. The results are shown in Figure 3a,b at various times for CO_2 and N_2, respectively. Note that every point on these

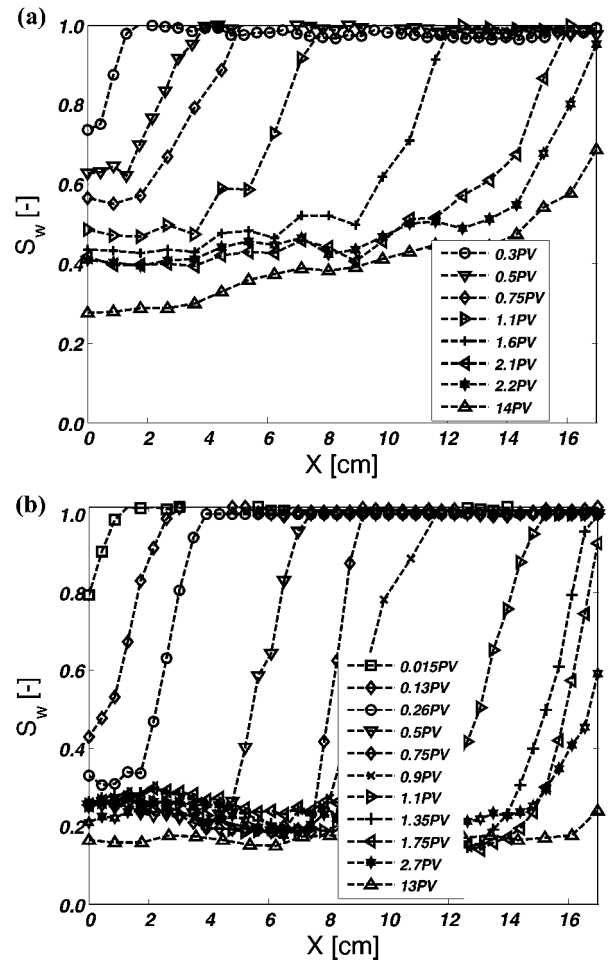

Figure 3. The liquid saturation profiles of (a) CO_2 foam and (b) N_2 foam, calculated from CT profiles shown in Figure 2.

Table 3. Amount of CO_2 that can be dissolved in water calculated from Henry's law at $P = 1$ bar and $T = 20$ °C. The solubility of CO_2 in water at this $P-T$ is estimated to be 38.4 mol/m^3

PV of CO_2 injected [−]	water content [cm^3]	amount of dissolved CO_2 (Henry's law) [cm^3]	PV of CO_2 dissolved [−]
0.30	2.6	1.2	0.06
0.50	7.5	3.4	0.16
0.75	10.4	4.8	0.23
1.10	15.6	7.2	0.34
1.35	21.6	9.6	0.47
1.60	26.8	12.4	0.59
1.90	30.5	14.1	0.67
2.10	36.5	16.8	0.80
2.20	40.2	18.5	0.92
breakthrough	42.5	19.6	0.93

figures is the averaged water saturation over a disk of the core with ~8 mm thickness. These figures show that foamed CO_2 and N_2 displace the liquid, that is, the surfactant solution from the porous medium. Prior to the gas breakthrough the saturation profiles along the core show a steep increase of S_w at the foam front, which indicates an effective front-like displacement of the initial liquid for both foams. In the case of CO_2 foam due to more fingering in the foam front, revealed by the CT images, the front is not as sharp as for the N_2 foam.

Another difference in the saturation profiles of these experiments (SAG scheme) with experiments reported in refs 26, 48 is the absence of so-called *secondary liquid desaturation* (SLD) stage in our experiments. The secondary liquid desaturation is driven by gas expansion and to be controlled by the competition between viscous and capillary forces.[26] Considering the differ-

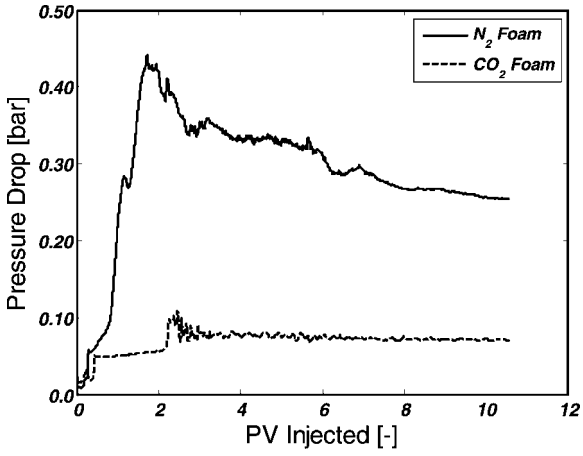

Figure 4. Pressure drop across the entire core for N_2 and CO_2 foam (q_g = 0.5 mL/min) at $P = 1$ bar and $T = 20$ °C.

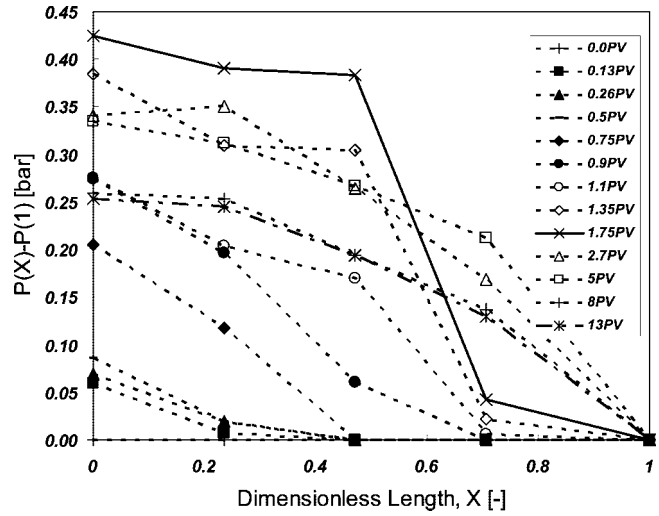

Figure 5. The transient pressure profile at different location in the core for N_2 foam experiment at $P = 1$ bar and $T = 20$°C.

ences in the experimental conditions, it seems that SLD is a phenomenon that happens in the experiments with high gas flowrates (and/or short cores).

The high values of liquid saturation at the region close to the core outlet indicates the capillary end effect where the porous medium retains the liquid in an attempt to maintain equilibrium across the outlet where the capillary pressure is zero or near zero.[49−51] After about 2 PV of gas injection, CO_2 foam removes about 50% of the liquid while N_2 removes more than 70% of the liquid. Further injection of N_2 after (foam) breakthrough removes the liquid retained at the inlet and outlet of the porous medium while further injection of CO_2 produces the liquid from the whole core as the liquid content is still high after foam breakthrough. Finally, comparing the water saturation profiles of two gases at the same pore volumes, one can conclude that the foamed N_2 displaces more liquid than foamed CO_2. Indeed, the foamed N_2 produces more than 82% of the initial liquid in the porous medium while the foamed CO_2 sweeps less than 65% of the initial liquid after more than 11 PV of gas injection.

c. Pressure Profiles. Figure 4 compares the measured pressure drops versus dimensionless time (PV) of the two experiments. It appears that the foamed N_2 builds up larger pressures over the core than foamed CO_2. The high liquid saturation and the small pressure drop indicate that CO_2 is in the form of relatively weak foam. Although this foam is relatively weak, it does produce a pressure drop higher than expected for the steady state pressure drop with the gas injection to a core initially saturated with water.[52] In both experiments the pressure drop across the core reaches a maximum and then declines slowly. The maximum point corresponds to the foam breakthrough at the outlet. The pressure decreases after breakthrough because of the coalescence of the bubbles due to diffusion or breaking of the foam films.

For a detailed explanation of foam progress in the core the pressure drop measurements at different sections of the core are plotted for the N_2 experiments in Figure 5. At early times, until 0.50 PV, the pressure drop is quite small. This means that foam is still weak. From time 0.50 PV to 0.70 PV there is a sharp increase in the pressure drop across the beginning of the core. This is confirmed by the saturation profile in Figure 3b. After 0.50 PV of gas injection, the foam front moves relatively slower along the core, nevertheless, it produces more water from the upstream region. Comparing the saturation profiles of two gases, this effect is more pronounced in the CO_2 foam, possibly because (i) CO_2 foam is weaker and (ii) unlike N_2 foam, the transition from weak to strong foam does not happen for CO_2. The low pressure drop and relatively high liquid saturation at the core inlet at early experimental times is referred to as the *entrance effect* in the literature.[29,35] Apparently gas needs time and space before it develops into foam. The pressure drop continues to increase as gas moves forward along the core. Again due to the capillary end effect the pressure drop at the last section of the core is low (water saturation is high). The pressure drop reaches maximum of 0.42 bar, which is equal to the overall pressure drop across the core. This means that foam in the last section is weaker than foam in the first half of the core. However, as it is seen from Figure 5 the pressure drop at the last section of the core increases with time indicating that foam becomes stronger with increasing amounts of injected gas. After foam breakthrough the pressure drop decreases due to the destruction of foam films as mentioned previously.

3.2. High Pressure Experiments. The second set of experiments were done at $P = 90$ bar and $T = 50$ °C. This $P-T$ condition is well above the critical point of CO_2.[53] The density of CO_2 is 286 kg/m^3 at this condition calculated from the Span and Wagner EoS.[54] Moreover, at this pressure and temperature, a water-rich liquid phase coexists with a CO_2-rich liquid, where a distinction between the vapor and liquid phases of CO_2 disappears.[55] Note that foams formed with dense CO_2 as the internal phase are strictly emulsions,[10] sometimes referred to as *foamulsion*.[5] However, for the sake of consistency we use the term foam here as well.

a. CT Images. Figure 6 presents the central CT images of CO_2 gas, CO_2 foam, and N_2 foam flow at $P = 90$ bar and $T =$ 50 °C. The time of each image is also shown in the dimensionless time of pore volumes, PV. The gas flowrate in these experiments was set to 1 mL/min. In the CO_2 gas experiment the core was initially saturated with brine, and CO_2 was injected into the core afterward. The images reveal the remarkable effect of the surfactant solution in the porous medium. When CO_2 is injected to the core initially saturated with the brine, there is no (clear) sharp interface between the gas and the brine. CO_2 forms channels through the brine and breaks through in less than 0.20 PV. When CO_2 is injected into the core initially saturated with the surfactant solution a clear interface between the moving gas and the liquid appears and CO_2 breakthrough is delayed until a time between 0.45 PV and 0.50 PV. The breakthrough time for N_2 foam is longer than 1.2 PV. Similar to the low pressure foam experiments the three regions are again present at high pressure foam experiments. In the CO_2 foam,

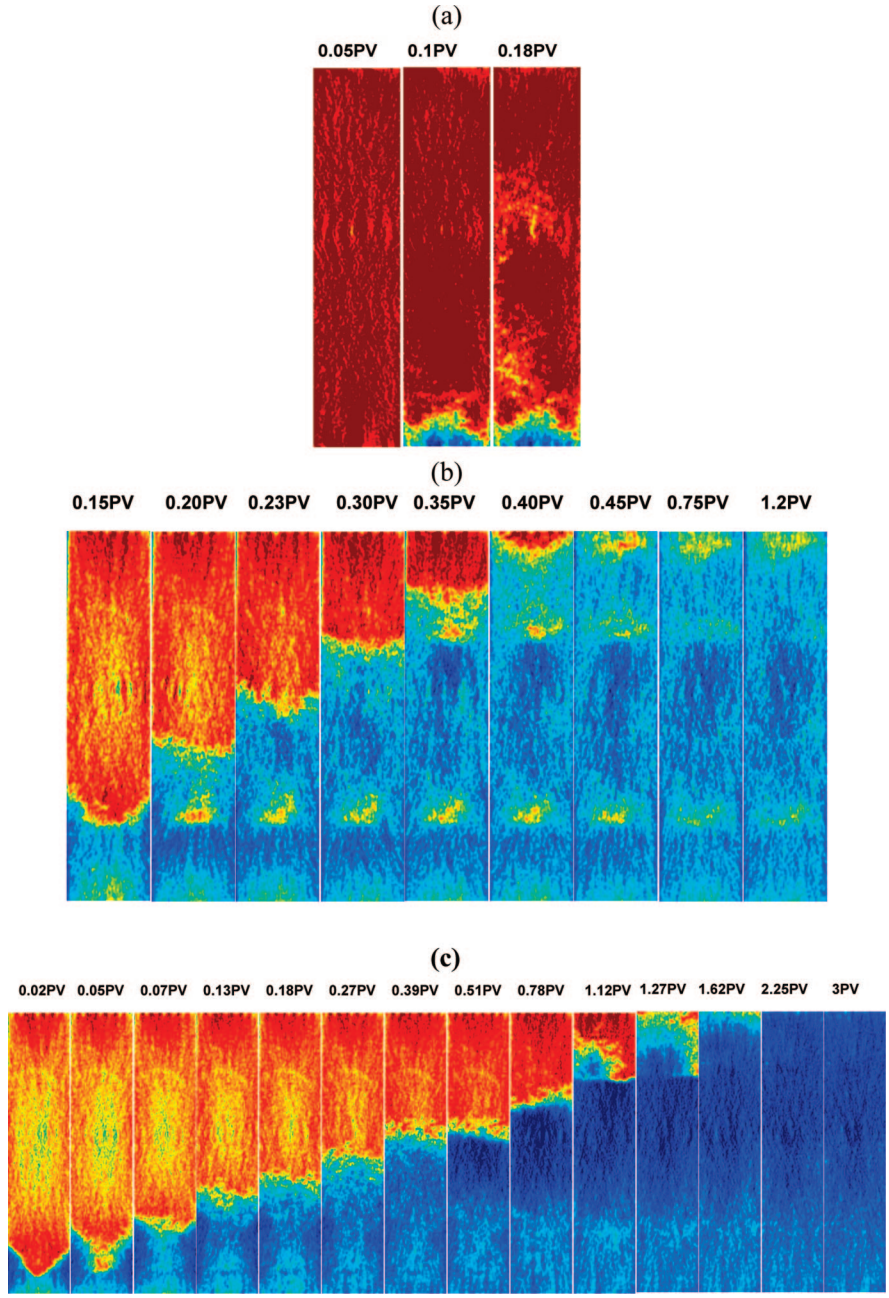

Figure 6. CT images of (a) CO_2 gas, (b) CO_2 foam, and (c) N_2 foam flow in a porous medium initially saturated with surfactant solution (red) at $P = 90$ bar and $T = 50$ °C ($q_g = 1$ mL/min). The time of each image is shown in pore volumes of the injected gas.

the gas bypasses part of the porous medium and therefore the brine content is high at regions near the core inlet and outlet. In the N_2 foam, the foam front moves a lot slower after 0.40 PV which is an indication that the foam has become stronger.

b. Pressure Profiles. Figure 7 shows the pressure history for CO_2 gas and CO_2 foam experiments while Figure 8 compares the pressure drop of CO_2 and N_2 foams. The pressure drop along the core follows a similar trend; it reaches a maximum at gas breakthrough and then declines with time. The maximum value of the pressure in CO_2 foam is about two times larger than that of CO_2 gas. Compared to the low pressure experiment, the pressure peak is higher at the high pressure CO_2 (and N_2) foam because (i) the gas flowrate is higher and (ii) CO_2 has a higher density (and viscosity) in the latter case. One interesting feature is that after 1.0 PV of CO_2 injection, the pressure drop of the CO_2 foam experiment is comparable to that of CO_2 gas experiment, meaning that after breakthrough there is almost no foam (or emulsion) present in the porous medium due to the shortage of the surfactant. The pressure drop for the N_2 foam is again larger than the CO_2 foam (see Figure 8). In the N_2 foam the pressure drop over the core is low until 0.40 PV, confirming the idea that gas should invade some part of the core before it develops into foam. This effect appears to be less significant for CO_2 than N_2 and as can be seen from Figures 2 and 6, the higher the gas flowrate the larger the entrance effect is.

c. Saturation Profiles. The calculated liquid saturation profiles, S_w, for the three experiments are shown in Figure 9. In all three experiments gas displaces the liquid, although when gas is foamed inside the porous medium the amount of the liquid that remains inside the core is less than when the gas is not foamed. Moreover, in the gas injection there is no steep increase of S_w at the gas front while in foam experiments an effective front-like displacement of the initial liquid by foam takes place. The capillary end effect is present in the experiments as the

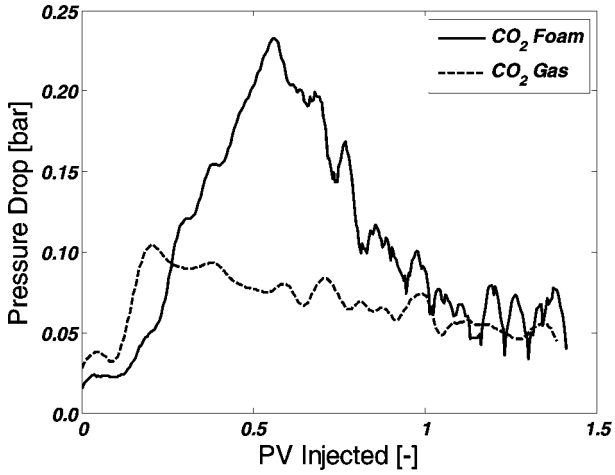

Figure 7. Pressure drop across the entire core for CO_2 gas and CO_2 foam (q_g = 1 mL/min) at P = 90 bar and T = 50 °C.

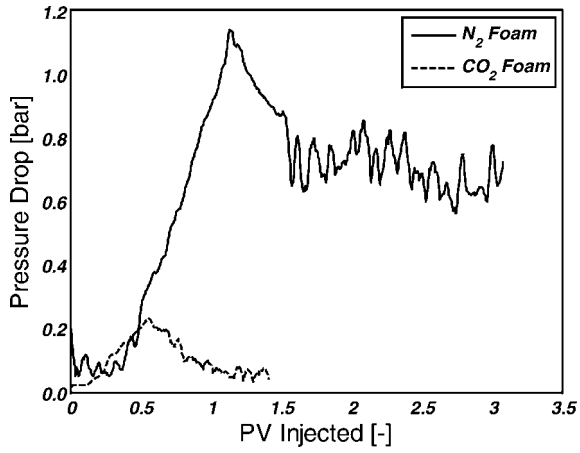

Figure 8. Pressure drop across the entire core for N_2 foam and CO_2 foam (q_g = 1 mL/min) at P = 90 bar and T = 50 °C.

liquid saturations are high near the core outlet. A detailed analysis of the N_2 foam experiments reveals that when the foam becomes stronger (after 0.40 PV of gas injection), the liquid saturation is reduced to a value as low as 8%; nonetheless due to the capillary end effects the saturation starts to increase to maintain the pressure equilibrium near the core outlet (This would have happened later if the core was longer). The SLD is present in this experiment because of the significance of the capillary end effects. After about 1.5 PV of gas injection, CO_2 gas produces about 40% of the initial liquid. Foaming of CO_2 increases the recovery by 25% and brings out more than 65% of the liquid. The N_2 foam removes more than 80% of the liquid.

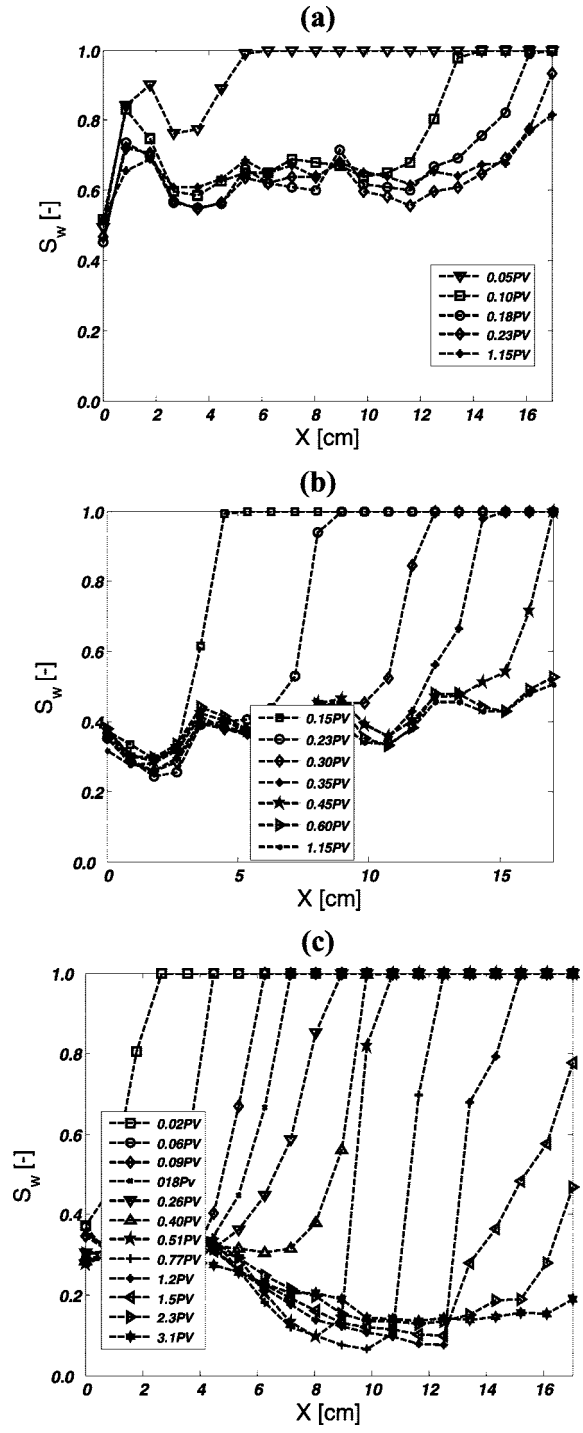

Figure 9. The liquid saturation profiles of (a) CO_2 gas, (b) CO_2 foam, and (b) N_2 foam, calculated from CT profiles shown in Figure 6.

4. General Discussion

The experiments in previous sections have clearly demonstrated that under a SAG scheme CO_2 foams are *weaker* than N_2 foams at both low and high pressures. Foam in porous media is considered *weak* when the number of the lamella is not large enough to resist the gas flow.[56,57]

To interpret these observations we need to recall that foams are thermodynamically meta-stable. They evolve irreversibly over time because the interfacial area in the lamella diminishes in order to minimize interfacial free energy.[58] The longevity of foam in porous media essentially relies on the stability of single foam films or lamellae. The stability of foam films depends on quantities and processes like surfactant concentration, salt concentration, adsorption kinetics, gravitational drainage, gas diffusion through foam films, surface forces (or capillary pressure) and fluctuations.[59,60] Before we assert the dominant factor responsible for the difference between CO_2 and N_2 foams it is worth reviewing how individual mechanisms could affect foam stability.

Coalescence and Drainage. These two processes are responsible for the changes in degree of dispersion of gas bubbles in foam as they cause (i) the diffusion of gas through the lamellae and (ii) collapse of liquid lamellae and subsequent coalescence of contiguous gas bubbles.[61] Pressure difference

between bubbles of unequal size induces gas-transfer from small to larger bubbles. Even in the ideal situation of an initially perfectly ordered foam, comprising uniform bubbles with a uniform gas pressure, finite size perturbation in bubble shape (e.g., due to irregularities and heterogeneity in porous media) would lead to an irreversible growth of the larger bubbles at the expense of the smaller.[56] This foam coarsening, the Oswald ripening, is unavoidable.[37]

The mass-transfer rate of gas through foam films can be characterized by the film permeability k. Following Princen and Mason[62] gas permeability depends on physical coefficients according to equation

$$k = \frac{k_H D}{h_w + 2D/k_{ml}} \tag{3}$$

where D is the diffusion coefficient of the gas in the liquid phase, k_H is the Henry's coefficient, k_{ml} is the permeability of the surfactant monolayer to gas, and h_w is the thickness of the liquid film. Equation 3 shows that the permeation rate for thick foam films, ($2D/k_{ml} \ll h_w$), is mainly controlled by the liquid layer via D and k_H ($k \sim k_H D$), while for thin foam films ($2D/k_{ml} \gg h_w$) the permeability of the monolayer ($k = k_H k_{ml}/2$) is the limiting factor.

The gas permeability of the foam films essentially depends on the solubility of the gas in the aqueous phase and the monolayer permeability. To compare the solubilities of the gases we may use the ratio of their their Henry's constants, $k_{H,CO_2}/k_{H,N_2} = 3.4 \times 10^{-2}/6.1 \times 10^{-4} = 55$. This implies that CO_2 is about 55 times more soluble in water than N_2.[46] In the only published data, the transfer rate of CO_2 through the foam films stabilized by hexadecyltrimethylammonium bromide (HDTAB) in the presence of NaBr was measured to be about 60 times larger than that of N_2.[62,67]

The rather good agreement between the two ratios (solubility and film permeability ratio) suggests that coalescence rate of CO_2 foam bubbles must be much higher than than that of N_2 foam bubbles. Therefore this could be why CO_2 foam is weaker than N_2 foam. This is analogous to the situation of steam foam where water vapor can pass through lamellae by condensing on one side and evaporating on the other side.[68] A small amount of nitrogen is added to reduce this effect in steam foam[69] and in the beer industry.[37,70] The higher solubility of CO_2 could also explain why in CO_2 foam more pore volumes of gas are needed before the gas becomes visible in the core and also why the speed of the foam front is lower for CO_2 than for N_2. Indeed a considerable fraction of CO_2 dissolved in the surfactant solution before can be foamed since the amount of available gas for foaming is reduced.

In porous media the Plateau borders are connected throughout the pore space and form a conductive network. In response to the local pressure gradient and gravity the liquid starts to flow. Liquid depletion in turn increases the capillary suction pressure on the lamella, which may result in film rupture. Coarsening also has a strong influence on foam drainage for gases of large solubilities (e.g., CO_2) and small bubble sizes (diameters < 1 mm).[63−66] This coupling effect can shorten the lifetime of (CO_2)-foam.

The lamellae remain in the pore throats of porous media and ideally at equilibrium they will have no curvature and thus sustain no pressure drop. Therefore in the absence of the driving force the diffusion process stops. This may cause the foam to remain *indefinitely* in the porous medium in the *absence of external disturbances* (in porous media heterogeneity and temperature fluctuations can be counted as external disturbances).[71,72]

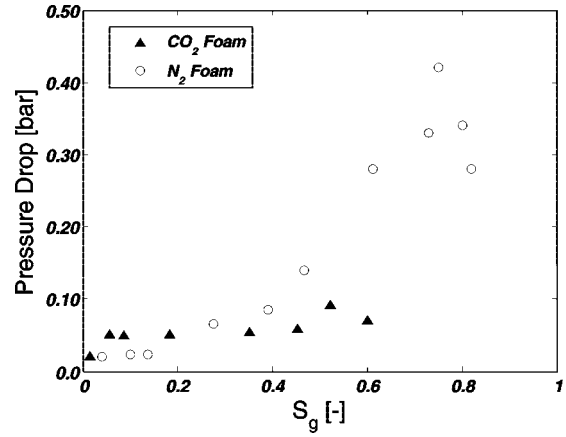

Figure 10. Pressure drop over the core vs average gas saturation in the core for low pressure experiments [$P = 1$ bar and $T = 20$ °C].

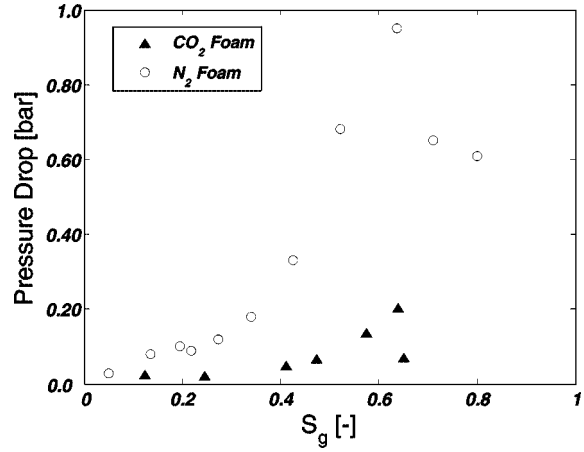

Figure 11. Pressure drop over the core vs average gas saturation in the core for high pressure experiments [$P = 90$ bar and $T = 50$ °C].

Figure 10 shows a plot of the pressure drop over the entire core as a function of the average gas saturation in the core for low pressure CO_2 and N_2 foams, respectively. Initially both foams show similar behavior, that is, while the gas displaces the liquid the pressure drop remains low (weak foam). However, as time passes for similar gas fractions (above $S_g = 0.30$), N_2 foam exhibits higher pressure drop over the core. This implies that (1) while a transition from weak foam to strong foam occurs in N_2 foam, CO_2 foam always remains weak, and (2) CO_2 foam is coarser than N_2 foam in porous media due to more intense rupture of the foam films (lamellae), as discussed previously. Figure 11 provides a similar plot for high pressure experiments. Again in this case there is a gas saturation in which the transition from weak foam to strong foam occurs in N_2 foam ($S_g \sim 0.35$). This saturation is higher than that of the low pressure N_2 foam presumably due to the differences in the flowrates. Seemingly, CO_2 continues to flow as a weak foam (or more accurately foamulsion) in the core.

Role of Interfacial Tension. The interfacial tensions of the CO_2-water and the N_2-water systems exhibit different behavior. The interfacial tension of the N_2-water binary system does not vary considerably with pressure such that it can be assumed constant in the range of our experimental pressures.[73,74] Nevertheless, the interfacial tension between CO_2 and water

depends strongly on pressure for pressures smaller than 10 MPa, decreasing as the pressure increases (from 72 to about 20 mN/m), and displays an asymptotic behavior toward a constant value for higher pressures.[75−77] Even at low pressure of 1 bar the presence of CO_2 above a surfactant solution may lower the interfacial tension possibly due to the surface hydrolysis of the surfactant.[78] The resistance to flow of the individual lamella in porous media is proportional to the surface tension.[79] It is interesting to mention that decrease in the interfacial tension leads to higher permeation of the gas molecules through the foam films and therefore may decrease the stability of foam.[80] Moreover, it has been observed that the relative permeability of CO_2 increases as the interfacial tension of the CO_2-water system decreases.[77]

Wettability Alteration Effects. Part of the observed differences in CO_2 and N_2 foam experiments may be attributed to both, differences in the interfacial tension and differences in the wetting angles of the two gases, that is, the value of $\sigma \cos \theta$, where σ is the gas−water interfacial tension and θ is the contact angle. Hildenbrand et al.[81] stated that for the N_2-water system the product of $\sigma \cos \theta$ exceeds the corresponding product for the CO_2-water system by a factor of 1.3−2.0. This suggests that wettability of the clay part of the rock may change with injecting CO_2. Foam is more stable in water-wet rock than in intermediate (or oil) wet porous media.[82−84] If the medium is not water-wet the walls may cause the lamellae to detach and collapse.[9] Our experiments are done in Bentheimer sandstone that contains 1−4 wt % of clay.[85] Therefore, injection of CO_2 affects the wettability of the cores. When the lamella moves across a nonwetting spot of the pores it ruptures by the pinch-off mechanism[35] lowering the resistance of foam to flow. It is important to remark that wettability and interfacial tension forces at the interface between liquid and rock may also affect bubble formation.[86] Hence, it is possible that the rate of foam generation in CO_2 foam is different than N_2 foam due to wettability effects.

pH Effects. Another factor that may affect the foam stability is the pH of the aqueous phase. When CO_2 is injected into a reservoir, CO_2 reacts with water and forms carbonic acid. This reaction may lower the pH of the brine down to 4.0.[87] The value of pH may influence the foam film stability by affecting the disjoining pressure through screening of the van der Waals and electrostatic forces.[60] The pH changes could also influence the surfactant performance in porous media.[88] However, based on the experimental results it has been asserted in the literature that pH has little effect on foam viscosity,[87] foam resistivity,[89] or in general foam stability when the surfactant concentration is above the CMC.[90]

Alteration of van der Waals Forces. The disjoining pressure is a measure of stability of a foam film and strongly depends on the film thickness.[58,61] According to the DLVO theory this pressure has two components: repulsive electrostatic and attractive van der Waals forces.[61] The effect of gas type on the van der Waals component of the disjoining pressure can be evaluated using Hamaker's constant, which depends on the optical and dielectric properties of the aqueous and nonaqueous phases.[91] Since these properties for CO_2 and N_2 are different it has been hypothesized that the differences in the magnitude of the attractive van der Waals forces of the lamellae in CO_2 and N_2 foams cause the differences observed in the experiments.[60] The calculations of ref 60 shows that the magnitude of screening of electrostatic forces for CO_2 is two times that of N_2, while screened Hamaker's constants indicate that van der Waals forces are six time lower for CO_2.

Type of Surfactant. Different gases may show different foaming behavior with different surfactants. Although AOS surfactants have been previously used in CO_2 foam projects, it is possible that type of surfactant is responsible for the differences observed in the experiments.

Temperature Effects. Temperature is another parameter that controls the foam stability by influencing the diffusion rate and adsorption of the surfactant molecules at the gas−water interface and rock surface. CO_2 dissolution in water is exothermic. The solution heat of CO_2 is given by

$$-(\mathrm{d} \ln k_H/\mathrm{d}(1/T))_{CO_2} = \Delta H_{CO_2}/R = 2400\ \mathrm{K} \rightarrow \Delta H_{CO_2} \approx 2.0 \times 10^4\ \mathrm{J/mol}$$

This implies that CO_2 dissolution can cause a temperature increase of

$$\Delta T_{CO_2} = \frac{\Delta H_{CO_2}}{k_H c_{p,w}} = \frac{2 \times 10^4}{3400 \times 4.2 \times 10^6} \approx 0.15\ \mathrm{K/bar}$$

A similar calculation for N_2 reads $\Delta T_{N_2} \approx 0.00015$ K/bar. Therefore, the temperature rise in the water due to CO_2 dissolution is more significant, especially at higher pressures. The increase in temperature can reduce the foam stability in porous media because (i) it can initiate the interbubble diffusion process by causing infinitesimal perturbation and thus disturbing the equilibrium and (ii) it increases the mass transfer rate through the bubbles. However, it should be noted that the temperature effects cannot completely be responsible for the differences in foaming behavior of CO_2 and N_2 since at low pressure the temperature effect will not be significant.

5. Conclusions

The foaming behavior of CO_2 and N_2 were comparatively studied in a sandstone core by the means of a CT scanner (X-ray). (C_{14}−C_{16})-Alpha Olefin Sulfonate (AOS) was used as surfactant. It has been shown that injection of a slug of surfactant prior to CO_2 injection can reduce the CO_2 mobility, below and above its critical point. The two investigated gases exhibit different behavior in the porous medium. Foaming of CO_2 builds up lower pressure drop over the core at both low and high pressures when compared to N_2. Both gases require space to develop into foam. The space is longer for N_2 (larger entrance effect) and increases with increasing gas velocity. The CT images and calculated water saturation profiles reveal that N_2 foam displaces the liquid in a front-like manner (sharp-vertical interface) while the propagation front for CO_2 foam is not the exact front-like displacement at low pressure. Moreover, the ultimate production by N_2 foam is always higher than by CO_2 foam. The observed differences in the foaming behavior of two gases can be related to the differences in their nature, mainly solubility in water, interfacial tensions, pH effects, type of surfactant, and the possible wettability effects. From these various factor solubility is likely the most critical one because (1) part of the gas is dissolved in the aqueous phase and, therefore, when volumetric flowrates of two gases are the same, the local gas velocities will be different, that is, the amount of available CO_2 for foaming will be lower than of N_2 at similar PVs, and (2) it significantly affects the gas permeability coefficient and, thus, the foam stability.

Acknowledgment

This research was carried out as part of the project funded by Delft Earth Research and Shell International Exploration and

Production, Rijswijk. We thank the technicians of the Dietz laboratory of our faculty for their support.

Literature Cited

(1) Klusman, R. W. *Energy Convers. Manage.* **2003**, *44*, 1921–1940.

(2) Holtz, M. H.; Nance, P. K.; Finley, R. J. *Environ. Geosci.* **2001**, *8* (3), 187–199.

(3) Koide, H.; Yamazaki, K. *Environ. Geosci.* **2001**, *8* (3), 218–224.

(4) Orr, F. M., Jr.; Heller, J. P.; Taber, J. J. *J. Am. Oil Chem. Soc.* **1982**, *59*, (10).

(5) Wellington S. L.; Vinegar, H. J. Surfactant-Induced Mobility Control for Carbon Dioxide Studied with Computerized Tomography. In *Surfactant Based Mobility Control—Progress in Miscible Flood Enhanced Oil Recovery*; Smith, D. H., Ed.;ACS Symposium Series 373; American Chemical Society: Washington, DC, 1988; pp 344−358.

(6) Blunt, M.; Fayers, F. J.; Orr, F. M., Jr. *Energy Convers. Manage.* **1993**, *34*, 1197–1204.

(7) Lake, L. W. *Enhanced Oil Recovery*; Prentice Hall: Englewood Cliffs, NJ, 1989.

(8) Fried, A. N. Foam drive process for increasing the recovery of oil. *Bureau of Mines Report of Investigation*. Bureau of Mines: Washington, DC, 1961.

(9) Rossen, W. R. Foams in Enhanced Oil Recovery. In *Foams:Theory Measurement and Applications*; Prud'homme, R. K., Khan S., Eds.; Marcel Dekker: New York City, 1996.

(10) Bond, D. C.; Holbrook, O. C. U.S. Patent No. 2,866,507, 1958.

(11) Kovscek, A. R.; Radke, C. J. Fundamentals of foam transport in porous media. In *Foams: Fundamentals and Applications in the Petroleum Industry*; ACS Advances in Chemistry Series, No. 242; American Chemical Society: Washington, D. C. 1994.

(12) Falls, A. H.; Hirasaki, G. J.; Patzek, T. W.; Gauglitz, D. D.; Miller, D. D.; Ratulowski, J. *SPE J.* **1985**, 176–190.

(13) Hirasaki, G. J. *J. Pet. Technol.* **1989**, *41*, 449–456.

(14) Krause, R. E.; Lane, R. H.; Kuehne, D. L.; Bain, G. F. Presented at the 8th SPE/DOE Symposium on EOR, Tulsam, OK, April 22−24, 1992; SPE 24191.

(15) Preuss, K.; Garcia, J. *Environ. Geol.* **2002**, *42*, 282–295.

(16) Nordbotten, J. M.; Celia, M. A.; Bachu, S. B.; Dahle, H. *Environ. Sci. Technol.* **2005**, *39* (2), 602–611.

(17) Rossen, W. R.; Gauglitz, P. A. *AIChE* **1990**, *36*, 1176–88.

(18) Chou, S. I. Presented at the SPE Annual Technical Conference and Exhibition, Dallas, TX, October 6−9, 1991; SPE 22628.

(19) Turta, A. T.; Singhal, A. K. Presented at the SPE International Conference and Exhibition, China, Beijing, November 2−6, 1998; SPE 48895.

(20) Svortol; Vassenden, F. Mannhardt, K. Presented at the SPE/DOE 10th Symposium on Improved Oil Recovery, Tulsa, OK, April 21−24, 1996; SPE 35400.

(21) Blaker, H. K. Celius, T.; Liet, H. A. Martinsen, L.; Ramsussen Vassenden, F. Presented at the SPE Annual Technical Conference and Exhibition, Houston, TX, October 3−6, 1999; SPE 56478 (SPE 78824).

(22) Aarra, M. G. Skauge, A.; Martinsen, H. A. Presented at the SPE Annual Technical Conference and Exhibition, San Antonio, TX, September 29−October 2, 2002; SPE 77695.

(23) Matthews, C. S. In *Enhanced Oil Recovery II, Processes and Operations*; Donaldson, E. C., Chilingarian, G. V., Yen, T. F., Eds.: Elsevier Science: New York, 1989.

(24) Heller, J. P. CO_2 Foams in Enhanced Oil Recovery. In *Foams: Fundamentals and Applications in the Petroleum Industry*; Schramm L. L. Ed.:ACS Advances in Chemistry, Ser. 3, No. 242; American Chemical Society: Washington, D.C., 1994.

(25) Huh; Handy, L. L. *SPE Reservoir Eng*. February 1989.

(26) Nguyen, P. Q. Dynamics of Foam in Porous Media. Ph.D. Dissertation. Delft University of Technology, The Netherlands, 2004.

(27) Du, D. X.; Naderi Beni, A.; Farajzadeh, R.; Zitha, P. L. J. *Ind. Eng. Chem. Res.* **2008**, *47*, 6298–6306.

(28) Nguyen, P. Q.; Currie, P. K.; Buijse, M.; Zitha, P. L. J. *J. Petrol. Sci. Eng.* **2007**, *58*, 119–132.

(29) Myers, T.; Radke, C. J. *Ind. Eng. Chem. Res.* **2000**, *39* (8), 2725–2741.

(30) Tortopidis, S.; Shallcross, D. C. Presented at the Asia Pacific Oil and Gas Conference, Australia, November 7−10, 1994; SPE 28811.

(31) Fergui, O.; Bertin, H.; Quintard, M. *J. Petrol. Sci. Eng.* **1998**, *20*, 9–29.

(32) Irani, C. A.; Solomon, C. Presented at the 5th Symposium on EOR, Tulsa, OK, April, 20−23 1986; SPE/DOE 14962.

(33) Raza, S. H. *Soc. Pet. Eng*. **1970**, *10*, No. 4.

(34) Wang, G. C. Presented at the4th Symposium on EOR, Tulsa, OK, April, 15−18, 1986; SPE 12645.

(35) Myers, T. The role of residual oil in the mechanistic simulation of foam flow in porous media: Experiment and simulation with the population balance method. Ph.D. Dissertation. University of California, Berkeley, 1999.

(36) Krastev, R. Private communication, 2008.

(37) Weaire, D.; Hutzler, S. *The Physics of Foams*; Oxford University Press: Oxford, U.K., 1999.

(38) Saint-James , L.; Langevin, D. *Condens. Matter Phys.* **2002**, *14*, 9397–9412.

(39) Kuhlan, M. I.; Falls, A. H.; Hara, S. K. Monger, T. G. Borchardt, J. K. Presented at the SPE/DOE Symposium on Enhanced Oil Recovery, Tulsa, OK, April 22−25, 1990; SPE/DOE 20192.

(40) Holm, L. W.; Garrison, W. H. *SPE Reservoir Eng.* **1988**, *3*, 112.

(41) Gauglitz, P. A. Friedmann, F.; Kam, S. I. Rossen, W. R. Presented at the SPE/DOE Improved Oil Recovery Symposium, Tulsa, Oklahoma, U.S., April 13−17, 2002; SPE 75177.

(42) Hutchins, R.D.; Miller, M. J. A Circulating Foam Loop for Evaluating Foam at Conditions of Use. *SPE Product. Facilities* **2005**, *20*, 286.

(43) Prieditis; Paulett, G. S. Presented at the SPE/DOE Eighth Symposium on Enhanced Oil Recovery, Tulsa, OK, 1992; SPE 24178.

(44) Farajzadeh, R.; Krastev, R.; Zitha, P. L. J. *Colloids Surf. A* **2008**, *324*, 35–40.

(45) Du, D. X. Private communication, 2007.

(46) Sander, R. *Compilation of Henry's Law Constants for Inorganic and Organic Species of Potential Importance in Environmental Chemistry*, version 3, 1999, p 57; http://www.mpch-mainz.mpg.de/%7Esander/res/henry.html (last date accessed September 2008).

(47) Brooks, R. A.; Weiss, G. H.; Talbert, A. J. *J. Comput. Assist. Tomog.* **1978**, *2*, 577.

(48) Zitha, P. L. J.; Nguyen, Q. P.; Currie, P. K.; Buijse, M. A. *Transp. Porous Media* **2006**, *64*, 301–313.

(49) Apaydin, O. G.; Kovscek, A. R. *Transp. Porous Media* **2001**, *43*, 511–536.

(50) Douglas, J. J.; Wagner, R. J. *Petrol. Transact., AIME* **1958**, *213*, 96–102.

(51) Perkins, F. M. J. *Petrol. Trans., AIME* **1957**, *210*, 409–411.

(52) Mahmoodi, N. Immiscible Foam for EOR. MSc. Thesis. Delft University of Technology, The Netherlands, July 2008.

(53) Poling, B. E.; Prausnitz, J. M.; O'Connell, J. P. *The Properties of Gases and Liquids*, 5th ed.; McGraw Hills: New York, 2000.

(54) Span, R.; Wagner, W. *J. Phys. Chem. Ref. Data* **1996**, *25* (6), 1509–1596.

(55) Spycher, N.; Pruess, K.; Ennis-King, J. *Geochim. Cosmochim. Acta* **2003**, *67* (16), 3015–3031.

(56) Heller, J. P.; Kuntamukkula, M. S. *Ind. Eng. Chem. Res.* **1987**, *26*, 318–25.

(57) Kibodeaux, K. R. Experimental and Theoretical Studies of Foam Mechanisms in Enhanced Oil Recovery and Matrix Acidization Application. Ph.D. Dissertation. University of Texas at Austin, Texas, 1997.

(58) Kornev, K. G.; Niemark, A. V.; Rozhkov, A. N. *Adv. Colloid Interf. Sci.* **1999**, *82*, 127–187.

(59) Klitzing, R. v.; Müller, H.-J.; *Curr. Opin. Colloid Interface Sci.* **2002**, *7*, 42−49.

(60) Aronson, A. S.; Bergeron, V.; Fagan, M. E.; Radke, C. J. *Colloids Surf. A* **1994**, *83*, 109–20.

(61) de Vries, A. J. *Foam Stability, A Fundamental Investigation of the Factors Controling the Stability of Foams*; Delft: The Netherlands, 1957; Communication No. 326.

(62) Princen, H. M.; Mason, S. G. *J. Colloid Sci.* **1965**, *20*, 353.

(63) Higenfeldt, S.; Koehler, S. A.; Stone, H. A. *Phys. Rev. Lett.* **2001**, *86* (20), 4704–4707.

(64) Gandolfo, F. G.; Rosano, H. L. *J. Colloid Interface Sci.* **1997**, *194*, 31–36.

(65) Vera, M. U.; Durian, D. J. *Phys. Rev. Lett.* **2002**, *88* (8), 088304-1−4.

(66) Maurdev, G.; Saint-Jalmes, A.; Langevin, D. *J. Colloid Interface Sci.* **2006**, *300*, 735–743.

(67) Princen, H. M.; Overbeek, J. T. G.; Mason, S. G. *J. Colloid Interface Sci.* **1967**, *24*, 125–130.

(68) Hirasaki, G. J. Private communication, 2008.

(69) Falls, A. H.; Lawson, J. B.; Hirasaki, H. J. *J. Pet. Technol.* **1988**, 95–104.

(70) Teng; Dokos, J. H. U.S. Patent no. 4610888, 1986.

(71) Cohen, D.; Patzek, T. W.; Radke, C. J. *J. Colloid Interface Sci.* **1996**, *179*, 357–373.

(72) Cohen, D.; Patzek, T. W.; Radke, C. J. *Transp. Porous Media* **1997**, *28*, 253–284.

(73) Masoudi, R.; King, A. *J. Phys. Chem.* **1974**, *78*, 2262–2266.
(74) Masterton, W. L.; Bianchi, J.; Slowinski, E. J. *J. Phys. Chem.* **1963**, *67*, 615–618.
(75) da Rocha, S. R. P.; Harrison, K. L.; Johnston, K. P. *Langmuir* **1999**, *15*, 2.
(76) Chiquet, P.; Daridon, J.-L.; Broseta, D.; Thibeau, S. *Energy Convers. Manage.* **2007**, *48*, 736–744.
(77) Bachu, S.; Bennion, B. *Environ. Geol.* **2008**, *54*, 1707–1722.
(78) Gilanyi, T.; Stergiopoulos, C.; Wolfram, E. *Colloid Polym. Sci.* **1976**, *254*, 1018–1023.
(79) Hirasaki, G. J.; Lawson, J. B. *SPE J.* **1985**, 176–190.
(80) Krustev, R.; Platikanov, D.; Nedyalkov, M. *Colloids Surf. A* **1997**, *383*, 123–124.
(81) Hildenbrand, A.; Schlomer, S. Kroos, B. M. Littke, R. *Geofluids* **2004**, *4*, 46161−46180.
(82) Suffridge, F. E.; Raterman, K. T.; Russell, G. C. *SPE* **1989**, 19691.
(83) Manhardt, K.; Novosad, J. J. *In Situ* **1994**, *18* (2), 145−183.
(84) Schramm, L. L.; Mannhardt, K. *J. Petrol. Sci Eng.* **1996**, *15*, 101–113.
(85) Al-Muntasheri, G. Polymer gels for water control: NMR and CT scan studies. Ph.D. Dissertation. Delft University of Technology, The Netherlands, 2008.
(86) Kogawa, H.; Shobu, T.; Futakawa, M.; Bucheeri, A.; Haga, K.; Naoe, T. *J. Nucl. Mater.* **2008**, *377*, 189–194.
(87) Fredd, C. N. Miller, M. J. Quintero, B. W. Presented at the SPE International Symposium and Exhibition on Formation Damage Control, Lafayette, Louisiana, February 18−20, 2004; SPE 86493.
(88) Radke, C. J. Private communication, 2008.
(89) Zhu, T.; Strycker, A.; Raible, C. J. Vineyard, K. Presented at the SPE/DOE Improved Oil Recovery Symposium, Tulsa, OK, April 19−22, 1998; SPE 39680.
(90) Liu, Y.; Grigg, R. B. Presented at the SPE International Symposium on Oilfield Chemistry, The Woodlands, TX, February 2−4, 2005; SPE 93095.
(91) Israelachvili, J. *Intermolecular and Surface Forces*; Academic Press: London, 1991.
(92) Farajzadeh, R.; Krastev, R.; Zitha, P. L. J. *Adv. Colloid. Interf. Sci* **2008**, *137*, 27–44.

Received for review November 18, 2008
Revised manuscript received February 16, 2009
Accepted February 26, 2009

IE801760U